Research Journal of Chemical Sciences ISSN 2231-606X
Vol. **14(1),** 31-44, February **(2024)** *Res. J. Chem. Sci.*

Isotherm and batch system kinetics of cadmium ion sorption using mango seed shell

Yusufu Luka, Abdulhalim Musa Abubakar*, Hassan Ahmed Saddiq, Solomon Isuwa
Department of Chemical Engineering, Faculty of Engineering, Modibbo Adama University, P.M.B 2076, Yola, Adamawa State, Nigeria
abdulhalim@mau.edu.ng

Available online at: www.isca.in, www.isca.me
Received 27th October 2023, revised 20th November 2023, accepted 1st January 2024

Abstract

Cadmium (Cd) toxicity even in low amounts can be felt if consumed by humans and animals. Mango seed shell biosorption property to get rid of this metal ion from contaminated water is therefore proposed by this study after several thoughtful bench-scale batch examination, beginning with Fourier Transform Infrared (FTIR) spectroscopic analysis. In that regard, the removal of Cd^{2+} at higher biosorption percentage occurs at low process conditions, which are: 10 min contact time, 0.5g biosorbent dose, 5mg/L initial Cd^{2+} concentration and pH = 4, corresponding to 82.47%, 99.49%, 62.43% and 62.45%, respectively. Uniquely, in this study, two solution approaches for finding isotherm model parameters from Langmuir, Freundlich and Dubinin-Radushkevich (D-R) formulae were also examined. Herein, the nonlinear regression technique (NRT) with satisfactory statistical estimates was the best method of finding the model parameters compared to the graphical technique (GT). Based on reduced chi-square, coefficient of determination (R^2) and the residual sum of squares (RSS) given by the user-defined NRT carried out in Origin Pro 2018, the best isotherm are in the order of Langmuir, D-R and Freundlich. Both techniques however, reveals that the adsorption of Cd unto mango seed shell endocarp is a physical adsorption process, due to an E = 0.3743 & 0.4677 kJ/mol obtained from the D-R isotherm. Also, an R^2 = 0.9978 from linear fitting, presents the Pseudo Second order adsorption kinetic model followed by the Lagergren alternative proposed in the literature, as the best model under the specified conditions. The bottom line now is to compare the biosorbent performance of mango seed shell with others reported previously and to determine the percent removal of other toxic heavy metals, also studying their isotherms and kinetics.

Keywords: Biosorption, Cadmium ion, Mango seed shell, Adsorption isotherm, Dubinin–Radushkevich, Intraparticle diffusion.

Introduction

Urbanization and industrial development saddled the environment with serious pollution concernworldwide[1], especially unwanted heavy metal above the World Health Organization (WHO) permissible limits discovered sometimes in drinking water[2,3]. Cadmium (Cd), as an example, is lustrous, ductile and soft, having silvery white color and is found in mineral form in form of Greenockite (Cd ochre) or byproduct of zinc[4–6]. Sources of Cd in the natural environment are as a result of natural phenomenon (e.g., erosion, weathering, river transport and volcanic eruption on land or ocean) and human activities including mining, improper disposal of cadmium-nickel (Cd-Ni) batteries, smelting and refining non-ferrous metals, tobacco smoking, combustion of fossil fuel and Cd-bearing or Ni-containing electronic wastes[6,7]. Health wise, Cdis toxic even at low concentrations in human bodies, causing reduced central nervous system function and potential blood, kidney, liver and lungs damage[8,9]. According to Mata et al., wastewater containing Cd is classified as "hazardous" if the concentration of Cd exceeds 1.0mg/L. An economical and environmentally-friendly means of getting rid of Cd or the biosorption technology, can be defined as the property of certain biomolecules (e.g., industrial wastes, bacteria, fungi, algae, yeast and agricultural wastes etc.) to bind and concentrate selected ions or other molecules from aqueous solution[10,11]. Biosorption gained precedence over other sorption techniques in the 1990s because conventional methods[12,13] are costly, less effective, and requires pretreatments coupled with other treatments[14]. In addition, biomass acting as biosorbent are often abundant in nature[15,16], have high metal removal efficiency, higher possibility of regeneration and re-utilization, less energy requirement and facilitates easier sludge handling[17]. The said conventional methods are precipitation[18–20], membrane separation[21–23], solvent extraction[24–26], ion exchange[27–29] and complexation[26,30].

According to Lazaridis & Asouhidou, the study of adsorption kinetics is very significant in order to determine the time required to reach equilibrium, develop predictive models for column experiments, and explore the parameters affecting the adsorption process. The parameters in question are contact time, pH, concentration and adsorbent dose. Methodological feasibility and cost-effectiveness are crucial factors in picking appropriate adsorbent to treat inorganic effluent.

Raval et al. mentioned the application of numerous adsorbents used for the exclusion of Cd ions from aqueous environment, including but not restricted to the use of activated carbon (charcoal, lignite, shell carbon), low-priced agricultural by-products (e.g., banana peels, rice bran, watermelon rind, nut shell, tea & coffee waste, straw, orange peel, mango shell, peat, dry tree leaves and barks, peanut shells, hull and saw dust), natural occurring materials (e.g., zeolite and clay), as adsorbents. Algae and some microorganisms may as well serve the same purpose of adsorbing Cd from solutions[23,32]. Mango is a tropical fruit found in eastern India[33] and the Northern states of Nigeria[34], consisting of seeds (endocarp) and peels (epicarp)[35,36]. Mango leaves powder can be used to remove Grey BL dye from aqueous solution[37]. Batch adsorption kinetics by Ashraf et al. and in a research paper by Iqbal et al., the possibility of adsorbing lead (II), Zn (II), Ni (II) and copper (II) ions have been studied.

Fourier Transform Infrared (FTIR) analysis revealed that hydroxyl and carboxyl groups within the adsorbent are the chief functional sites taking part in the process, also in Kowanga et al. Thus, this study is tailored towards examining the feasibility of using mango seed shell endocarp as adsorbent to sorption Cd (II) ions in a batch system from aqueous solutions. Specifically, the study sought to: prepare an adsorbent from mango seed shell endocarp by oven drying and grinding into powder, determine the effect of time, adsorbent dosage, and temperature on sorption of Cd ion in the batch system and determine the sorption kinetics and sorption isotherms parameters of the batch system.

Aninstantaneous equilibrium is established between adsorbed metal ions and adsorbent during adsorption. The most extensively used isotherm equation for modeling the equilibrium is the Langmuir equation which is effective for monolayer sorption unto a surface with a finite number of matching sites. Apragmatic Freundlich model also studies mono molecular layer handling of solute by the adsorbent even thoughit assumes the adsorbent has a heterogeneous surface so that binding sites are not alike[41]. In divergence to the Langmuir model, Freundlich isotherm make available no info on the monolayer adsorption capacity[42]. Langmuir and Freundlich isotherms constants are inadequate to clarify the physical and chemical characteristics of the adsorption process.

As a solution, the mean adsorption energy (E) calculated from the Dubinin–Radushkevich (D-R) isotherm provides important information about these properties, in addition to being used to describe the adsorption isotherms of single solute systems[40]. We therefore target the forgone isotherm models to calculate the equilibrium Cd uptake, q_e onto mango seed shell endocarp, applying both linear graphical method and a method of regression using relevant analytical computer application. The work is analogous to Ahmet & Mustafa's study on the adsorption performance of Cd (II) from aqueous solution onto red algae, where they realized that the adsorption progression is a function of the parameters such as solution pH, adsorbent dose, contact time, initial Cd (II) concentration and temperature. In addition, the prediction of adsorption rate gives important information for designing batch adsorption systems[3]. Kinetics of adsorption can be studied by means of 3 kinetic models, namely: Lagergren Pseudo-First-Order, Second order and the intra particle diffusion (IPD) models. Therefore, all these items form part of the objectives of this work.

Materials and Methods

Materials and Chemicals: Materials such as fresh mango seed shell (endocarp), deionized water, distilled water and Cd sulphate stock solution were used in this empirical study. Tools or equipment including, oven, mortar and pestle, orbital shaker, atomic absorption spectrophotometer (AAS) and plastic bottles were also utilized in conjunction with the chemicals and materials listed at various stages of the experiment.

Adsorbent Preparation: Fresh and ripe mango (*Mangifera indica*) seed was obtained from fruit sellers around Sangere and Sabon Gari axis of Modibbo Adama University (MAU), Yola in Nigeria. Removal of the seed shell was carried out followed by its washing with distilled water. It is followed by rinsing with deionized water, which was then used to rinse the seed shell before drying in an oven at 70°C for 48-72h, until a constant weight is observed. Next step involves drying the biomaterials and grinding it using mortar and pestle before storing in an airtight plastic bottle for further use as biosorbent.

Preparation of Metal Bearing Solutions: Stock solution of Cd was prepared using deionized distilled water with analytical grade cadmium sulphate heptahydrate ($CdSO_4.7H_2O$). All working solutions of varying concentrations were obtained by diluting the stock solution with distilled water. The pH of the solutions was then adjusted to 4.5 to prevent hydrolysis. To prepare the stock solutions with 100mg/L of the metal, 439.6 mg $CdSO_4.7H_2O$ was dissolved in 1000mL water.

Biosorption Study: Time Dependent Biosorption: Here, time-dependent batch and shake experiments were performed using a procedure reported previously by Ashraf et al. with minor modifications. The time intervals chosen for the time dependence studies were 10, 30, 60, and 120min. Next, 5mg/L was chosen as the metal concentration of the treatment solutions. Regarding the shaking device, 200 rpm was specified as the speed of the orbital shaker and a temperature of 32^{o}C was set.

Dose Dependent Biosorption: As contained in Ashraf et al. the biosorbent dose dependent batch and shake experiments were performed; however, with minor modifications. The sorption of metals at biosorbent concentrations of 0.5g, 1g, 1.5g, and 2g were carried out. Since an optimum time had been found, speed of the orbital shaker was set at 200rpm to run the shake experiment. Temperature was set at 32^{o}C and the metal concentration of the treatment solutions chosen was 5mg/L.

Metal Concentration Dependent Biosorption: Ashraf et al. previously described the metal concentration dependent batch and shake experiments. Similar approach was followed with minor modifications. At a fixed biosorbent concentrations of 1.5g sorption of metal concentrations of 2.5, 5.0, 50, 100 mL was carried out. Time was kept constant at 120 min optimal value as well as speed of the orbital shaker for the shake experiment which was maintained at 200rpm. Metal concentrations of the treatment solutions was selected to be 5 mg/L, set at 32°C.

pH Dependent Biosorption: pH dependent batch and shake experiments was performed. The procedure was partly in accordance with Ashraf et al. with slight modifications. A pH of 3, 4, 4.5 and 5 were specified for the study. Metal concentration of the treatment solutions chosen was about 5mg/L. Speed of orbital shaker was kept at 200rpm for the shake experiment. This procedure was repeated in quadruplicate for the two biosorbents.

Estimation of Cd ion Concentration: Cadmium concentration after each test was determined via atomic absorption spectroscopy (AAS).

Statistical Analysis: All the experiments were performed in quadruplicate and data were presented as mean of the 4 experimental values. Microsoft Excel 2016 software was used to carry out the analysis. Several graphical plots were used to illustrate variations in adsorbent behaviour with changes in operating conditions.

Adsorption Isotherm: During adsorption, a rapid equilibrium is established between adsorbed metal ions and the adsorbent[43]. For a known initial (C_i) and final/equilibrium concentration (C_e), volume of the solution (V) and mass of the dry adsorbent (M), the equilibrium metal uptake (q_e) was first calculated using Equation-1[44].

$$q_e = \frac{(C_i - C_e)V}{M} \quad (1)$$

Taking known sets of $q_e$and sets of calculated C_e determined experimentally, adsorption isotherm parameters of three models, namely: Langmuir, Freundlich and Dubinin–Radushkevich (D-R) isotherms were determined.

Langmuir Isotherm Parameters: The Langmuir model is given by Equation 2[45]. Its constant parameters, q_{max} = maximum amount of the metal ion per unit weight of the adsorbent that will form a complete monolayer on the surface bound at high C_e and b = constant related to the affinity of the binding sites, were determined from the linear plot of $\frac{C_e}{q_e}$ versus C_e, based on Equation-3.

$$q_e = \frac{q_{max}\, b\, C_e}{1 + b\, C_e} \quad (2)$$

$$\frac{C_e}{q_e} = \frac{C_e}{q_{max}} + \frac{1}{b\, q_{max}} \quad (3)$$

Equation-3 is basically the linearized form of Equation 2 or the Langmuir isotherm.

Freundlich Isotherm Parameters: Equation 4 is the empirical Freundlich model consisting of K and n Freundlich constants characteristic of the system[42]. They are indicators of adsorption capacity and adsorption intensity, respectively.

$$q_e = K C_e^{\,1/n} \quad (4)$$

K can be determined from the intercept of the linear plot of Equation 5 and n, from the slope of the graph.

$$\log q_e = \log K + \frac{1}{n} \log C_e \quad (5)$$

Dubinin–Radushkevich Isotherm Parameters: D-R isotherm commonly used to describe the adsorption isotherms of single solute systems and as given by Equation 6 found in Kowanga et al. was used to determine q_{max} and B in the model. Linearizing the model, Equation 7 was formed, whose slope is −B and intercept = $\ln q_{max}$.

$$q_e = q_{max} \exp\left[-B\left(RT \ln\left[1 + \frac{1}{C_e}\right]\right)^2\right] \quad (6)$$

$$\ln q_e = \ln q_{max} - Be^2 \quad (7)$$

Still the model parameters, B = a constant related to the adsorption energy and q_{max} defined earlier can still not be determined if set of the independent variable 'e' in Equation is not known. Hence, Equation 8 where R = gas constant = 8.314 $\times 10^{-3}$kJ/mol.K and T = absolute temperature was used. T was already specified in the methodology.

$$e = RT \ln\left(1 + \frac{1}{C_e}\right) \quad (8)$$

Finally, a plot of $\ln q_e$ against e^2 was made to determine the D-R constants B and q_{max}. Note that 'e' is called the D-R model variable.

Parameter Determination Approaches: Two approaches were used to estimate the unknown isotherm model parameters. Method A: Model parameters was determined using linearized versions of the 3 isotherm models, from slopes and intercepts of the respective plots. Method B: Initial guesses based on typical range of values of the unknown parameters was made to fit q_e versus C_e plots, thereby estimating them via nonlinear regression in ORIGIN Pro software. Methods A and B were then compared to select the most accurate estimated parameters based on fitted plots. Method A is termed in this study as the Graphical Technique (GT) while Method B is the Nonlinear Regression Technique (NRT).

In order to determine the parameter 'E' in D-R model so as to distinguish whether the adsorption process is a physical or chemical process, Equation-9 was used finally.

$$E = \frac{1}{(2B)^{0.5}} \quad (9)$$

Adsorption Rate Predictions from Kinetic Models: Kinetics of adsorption was studied by using 3 kinetic models, namely; Lagergren Pseudo-First-Order, Second order and intraparticle diffusion (IPD) models, given by Equations 10-12 respectively[42].

$$\frac{dq_t}{dt} = k_1(q_e - q_t) \quad (10)$$

$$\frac{dq_t}{dt} = k_2(q_e - q_t)^2 \quad (11)$$

$$q_t = k_d t^{\frac{1}{2}} \quad (12)$$

Where, q_t = adsorption capacity at time, t (mg/g), k_1 = equilibrium rate constant of the Pseudo-First-Order adsorption process (min^{-1}), k_2 = second order rate constant (g/mg min) and k_d = intraparticle diffusion rate constant (mg/g $min^{-½}$). To determine the unknown parameters, Equations 10 and 11 for the First and Second order kinetics were linearized to give Equations 13 and 14[45], while Equation 12 requires no linearization.

$$\log(q_e - q_t) = \log(q_e) - \frac{k_1}{2.303}t \quad (13)$$

$$\frac{t}{q_t} = \frac{1}{k_2 q_e^2} + \frac{t}{q_e} \quad (14)$$

A table of values for $\log(q_e - q_t)$, $\frac{t}{q_t}$ and $t^{\frac{1}{2}}$ was then generated based on known experimental q_t and t, to estimate k_d, k_1, q_e and k_2 from slopes and intercepts of Equations-12-14 respectively. But first, a time-dependent rate study data involving q_t and t was generated. Unsatisfactory plot and parameter estimate using Lagergren-Pseudo-First-Order (A) model was checked and corrected using an alternative or Lagergren B model suggested by Sahoo & Prelot. It is given by Equation-15.

$$\frac{1}{q_t} = \left(\frac{k_1}{q_e}\right)t + \frac{1}{q_e} \quad (15)$$

Microsoft Excel 2016 was seriously employed in this section, where the coefficient of determination (R^2) for the respective fits were also obtained.

Results and Discussion

FTIR Spectrophotometry: In order to ascertain the adsorptive ability of the mango shell seed, FTIR examination carried out before and after absorption, result in Figures-1 and 2.

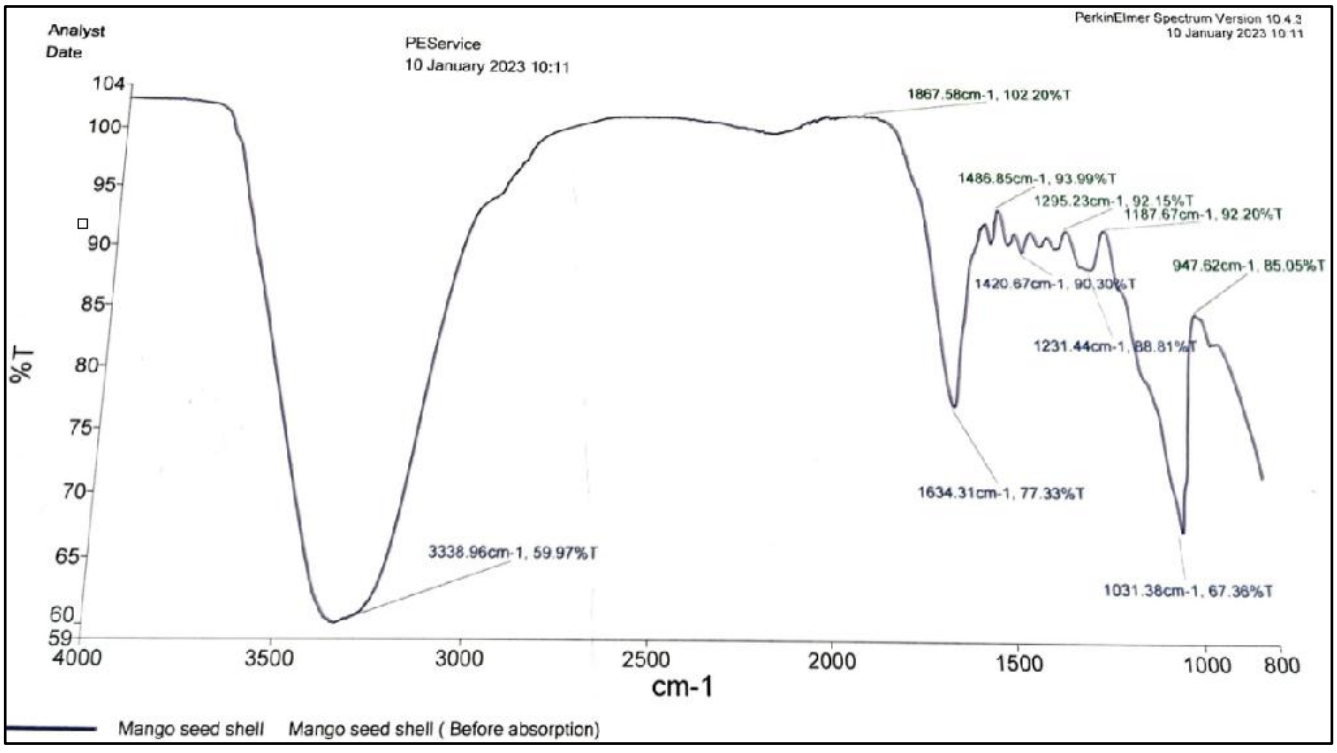

Figure-1: Mango Seed Shell FTIR Study before Adsorption.

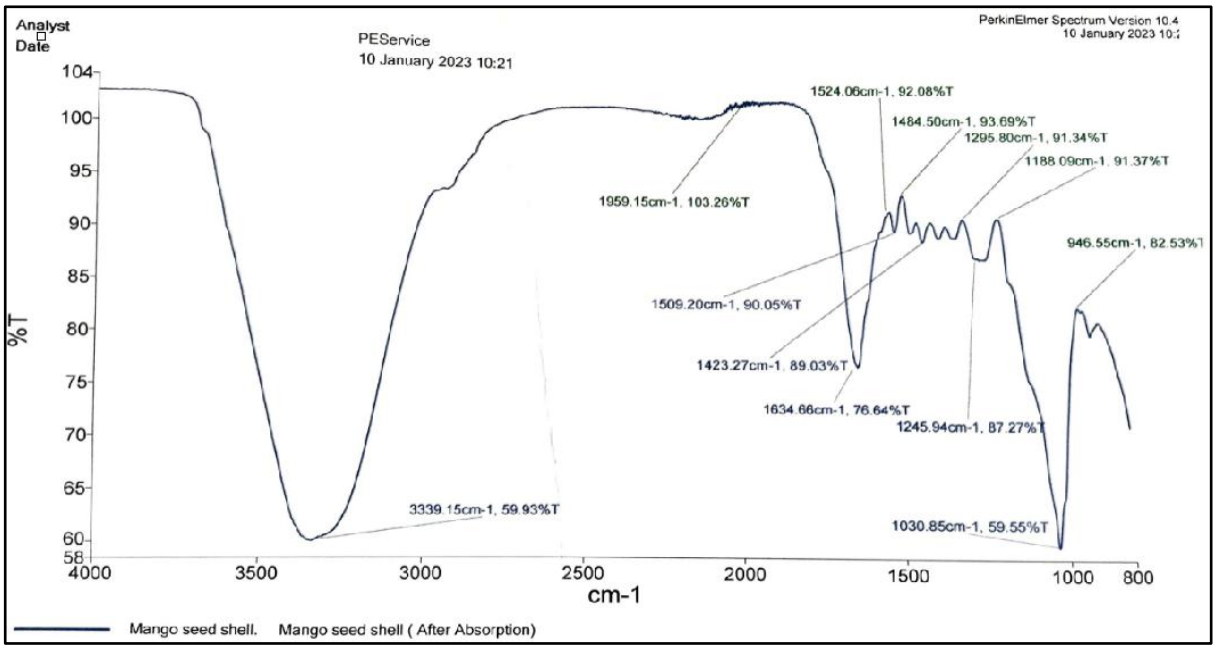

Figure-2: Mango Seed Shell FTIR Analysis after Adsorption.

The FTIR spectrum of untreated mango seed shell (Figure-1) point to the strong peak of hydroxyl (O–H) group at wave numbers of 3338.96, 1867.58, 1486.85, 1295.22, 1187.67, 1420.67, 947.62, 1231.44, 1634.31 and 1031.38cm^{-1}.

This implies that the assigned functional group (O-H), aliphatic amines, alkyne group and alkene group, denotes aldehydes, ketonic group and aromatic C-H bonding. Whereas, FTIR spectrum after absorption (Figure-2) show a shift in cadmium functional group, which shows that absorption took place.

Percent Biosorption at Varying Time and Dose: Table-1 shows how the percentage biosorption varied with time for a given biosorbent dose, metal concentration and mixing speed. On the other hand, Table-2 presents how the biosorption with mango seed shell endocarp vary with change in the biosorbent dosage.

Table-1: Variation of Percentage Biosorption with Time.

Time (min)	Initial Concentration (mg/L)	Final Concentration (mg/L)	% Biosorption
10	5	0.88	82.47%
30	5	1.37	72.66%
60	5	1.52	69.63%
120	5	1.88	62.43%

Table-2: Variation of Percentage Biosorption with Dosage.

Dose (g)	Initial Concentration (mg/L)	Final Concentration (mg/L)	% Biosorption
0.5	5	0.03	99.49%
1	5	1.67	66.56%
1.5	5	1.88	62.43%
2	5	2.57	48.70%

From Table-1, it can be seen that adsorption rate decreases with increase in time up to a minimum biosorption percentage equivalent to 62.43%. It indicates that, longer duration of the batch experiment is not likely to give higher percentage adsorption. Figure-3 depicts the plot of biosorption versus time.

Similarly, the plot shows that biosorption varies almost linearly with time and longer time might not be required for higher biosorption percentage. Essentially, the initial fast rate of metal sorption in the sample may be linked to large number of sorption sites available at the time. Afterwards, it is expected that the unsaturated sorption sites available becomes minimal due to decreasing steady rate of adsorption. This behavior reflects the fact that the adsorption is a surface phenomenon and that the surfaces are readily accessible to the metal ions in the solution[37]. Longer contact time will be needed to ascertain the expected theoretical decline of biosorption with mango seed shell endocarp. Also observed is that Table-2 Cd ions biosorption decreases with increase in adsorbent dose – as illustrated using Figure-4.

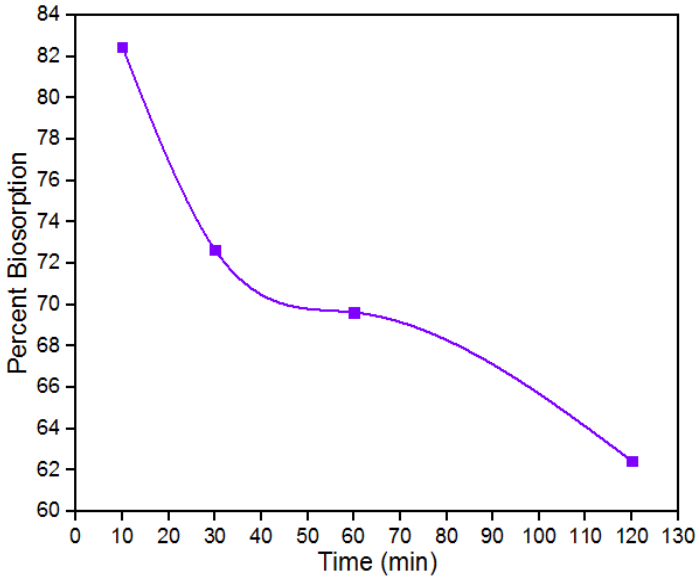

Figure-3: Variation of Percentage Biosorption with Time.

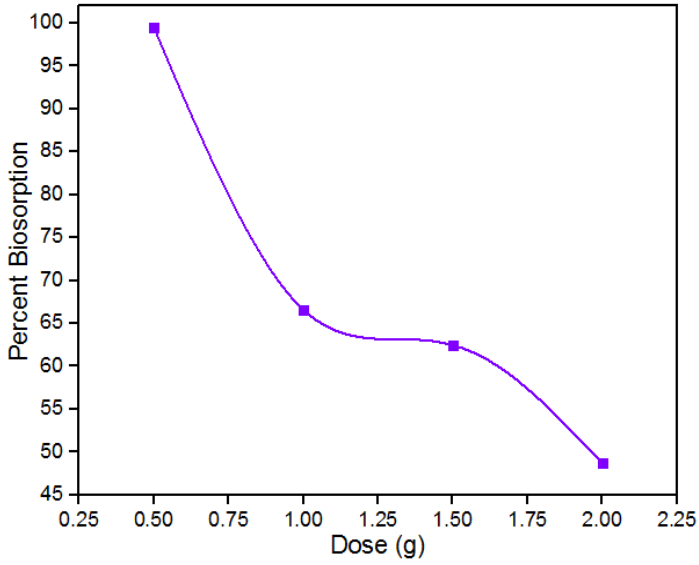

Figure-4: Percent Biosorption versus Dosage Variation.

Percent biosorption of Cd ion (Cd^{2+}) was optimal at 0.5g of adsorbent used (Table-2). Availability of larger surface area and more sorption sites is typical of a low biosorbent mass (dosage). Thus, the removal of Cd^{2+} was found to decrease with increase in biosorbent dosage, as evident in Figure-4. At a very low adsorbent concentration, the adsorbent surface becomes saturated with the metal ions and the residual metal ion concentration in the solution becomes large.

Biosorption Rate at Different Cd^{2+} Initial Concentration and pH: Table-3 shows the results of the metal concentration-dependent biosorption study while Table-4 displays that of the pH variation between 3-5.

Table-3: Initial Metal Concentration Variation Effect on Adsorption.

Initial Concentration (mg/L)	Final Concentration (mg/L)	% Biosorption
2.5	1.12	55.04%
5	1.88	62.43%
50	27.25	45.51%
100	70.92	29.08%

Table-4: Aftermath of the pH-Dependent Biosorption Experiment.

pH	Initial Concentration (mg/L)	Final Concentration (mg/L)	% Biosorption
3	5	1.93	61.49%
4	5	1.88	62.45%
4.5	5	1.88	62.43%
5	5	1.95	60.94%

For better visualization and understanding of the relationships between the initial Cd^{2+} concentration and pH, results in Tables-3 and 4 were graphically illustrated using Figure-5.

Table-3 shows the initial and final concentrations of the samples, corresponding to 2 h contact time, 1.5g adsorbent mass, 4.5 pH and 32^{o}C temperature. In line with this, the effect of initial metal ion concentration on the sorption of Cd^{2+} from the sample onto mango seed endocarp is represented in Figure 5a. The percentage removal of the Cd^{2+} from the effluent sample was found to increase steadily with increase in the initial Cd^{2+} concentration. The maximum adsorption (62.43%) occurs at 5 mg/L initial amount of the Cd^{2+}. The decrease with initial concentration may be due to the fact that at lower concentration of metal ions, almost all the active sites on the biomass are occupied and further increase in the initial Cd^{2+} concentration would only lead to supersaturation of biomass surface. An increase in % biosorption with increase in initial concentration implies that little of the Cd^{2+} were adsorbed at low concentration and the sorption sites are still available. Meanwhile, Table-4 and Figure-5b go hand-in-hand. It can be observed from Table-4 that the % removal of Cd is maximum at pH range of 4-4.5.

Isotherm Constant Parameters: Careful use of Equations 1 and 8, based on known concentrations (C_i and C_e) from Table-3 and T= 32^{o}C (307K), R = 8.314× 10^{-3} kJ/mol K, V = 19.94565 L and M = 1.5g, the generation of q_e and 'e' values in Table-5 became possible.

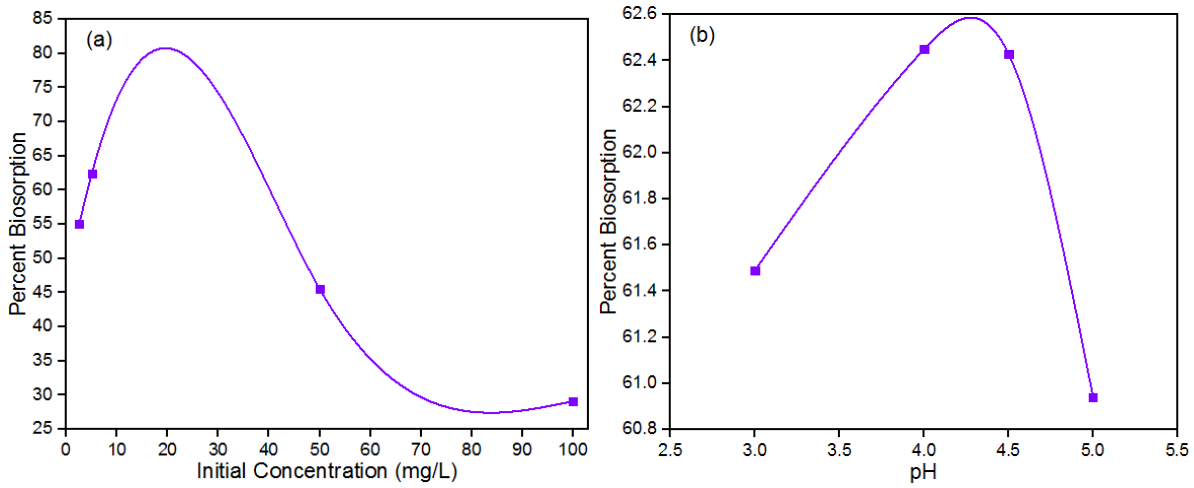

Figure-5: Plot of Percentage Biosorption versus (a) Metal Concentration and (b) pH.

Table-5: Variables for the Proposed Adsorption Isotherms.

C_i (mg/L)	C_e (mg/L)	q_e (mg/g)	e (mol/kJ)
2.5	1.12	18.35	1.62865
5	1.88	41.48695	1.08865
50	27.25	302.509	0.09199
100	70.92	386.6797	0.03574

These variables (C_i, C_e, q_e and e) can then be used to estimate model parameters for Langmuir, Freundlich and D-R isotherms using nonlinear regression analysis or from intercepts and slopes of a simple linear plots of Equations 3, 5 and 7 respectively.

Graphical Technique: Linear graphical representation of the model facilitates the estimation of the model parameters from intercepts and slopes obtained by plotting dependent and independent variables in Tables-5 and 6.

Table-6: Dependent and Independent Terms Values in Linearized Isotherm Equations.

Ce/qe (g/L)	log qe	log Ce	e^2 (mol^2/kJ^2)	ln qe
0.061035	1.263636	0.049218	2.652511	2.909629
0.045315	1.617912	0.274158	1.185148	3.725379
0.09008	2.480738	1.435367	0.008462	5.712111
0.183408	2.587351	1.850769	0.001277	5.957597

Regardless of whether the models were linearized using natural or common logarithms, the estimated results (Figures-6-8) are satisfactory. It is worthy of note that these logarithmic values are dimensionless.

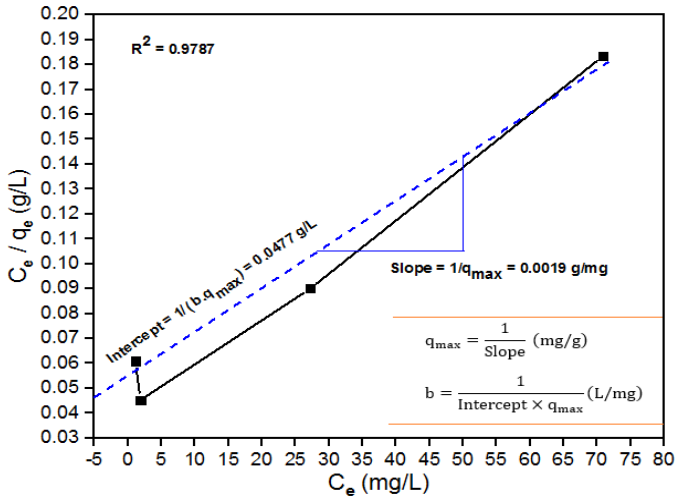

Figure-6: Determination of Langmuir Model Parameters Graphically.

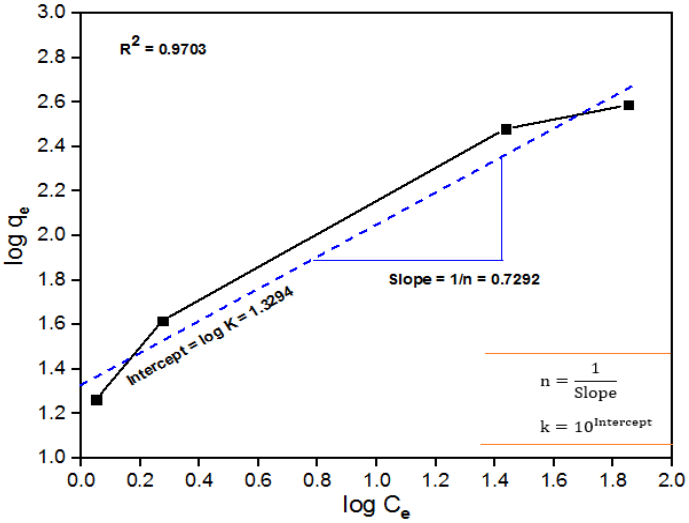

Figure-7: Determination of Freundlich Model Parameters Graphically.

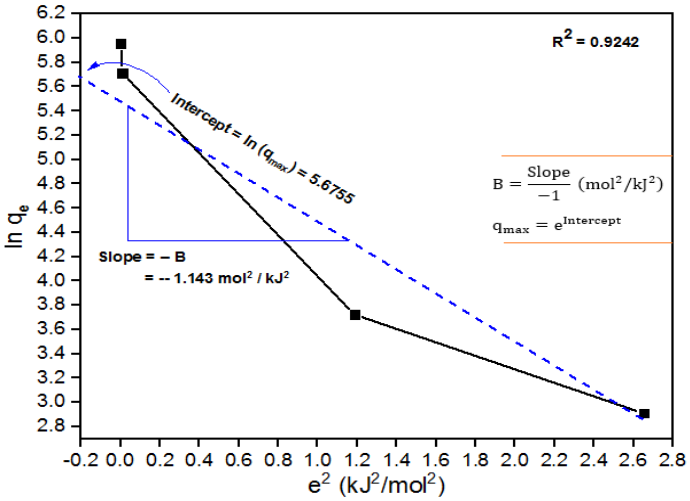

Figure-8: Determination of D-R Model Parameters Graphically.

A summary of the 3 models parameters determined using GT are shown in Table-7. Since none of the graphical illustrations are linear, the Excel graphing features used, gives those blue-dash linear lines shown in Figures-6-8.

The lines were drawn because the data were originally from the linearized versions of the model and thus, as expected, the given points on each graph must be joined to give a straight line. GT is not always reliable as specific values of the intercepts and slope may be difficult to determine. It is also obvious that R^2 obtained based on the variations in fittings of the experimental and the imaginary lines is near 100%. It shows that only 2.13% of the points are away from the thick line under Langmuir isotherm graph. Exactly 2.97% and 7.58% of the data points are unfitted under Freundlich and D-R isotherms respectively, as shown in Figures-7 and 8. In practical sense, finding isotherm parameters graphically is a lengthy procedure, even with Excel Spreadsheet. However, it is far more reliable than manual use of pencil and graph sheet, which requires adequate approximations to be able to represents every point on the graph axes.

Nonlinear Regression Technique: Equations 2, 4 and 6 are nonlinear and hence could serve as a User-Define model in ORIGIN software to help predict q_e that is approximately equal to the observed q_e in Table-5. By specifying initial guesses: q_{max} = 100 & b = 0.1 for Langmuir; K = 10 & n = 1 for Freundlich and; q_{max} = 100 & B = 1, the predicted q_e is as shown in Table-8.

In Table-8, the q_e for the GT as well as the one calculated using Equation 1 (termed 'experimental'), is shown for the sake of analogy. As seen, only handful of predicted q_e values using NRT are closer to the empirical values. The differences are therefore more illustrative if the variables are jointly plotted, as depicted in Figure-9.

Table-7: Isotherm Parameters Obtained Using GT (or Method A).

Model	Parameters					
	q_{max} (mg/g)	b	n	K	B	E
Langmuir	526.3158	0.039832	-	-	-	-
Freundlich	-	-	1.371366	21.3501	-	-
Dubinin–Radushkevich	291.6341	-	-	-	1.143	0.4676

Table-8: Predicted Equilibrium Cd^{2+} Uptake for all Models Using NRT.

qe (mg/g)						
Experiment	Langmuir		Freundlich		D-R	
	GT	NRT	GT	NRT	GT	NRT
18.35	22.47717	28.94265	23.18941	49.94801	14.06487	3.064086
41.48695	36.66694	46.70434	33.83108	64.96369	75.25451	41.99513
302.509	273.9372	295.5692	237.7218	252.3255	288.827	342.6759
386.6797	388.7128	390.5208	477.5077	409.9865	291.2087	347.0965

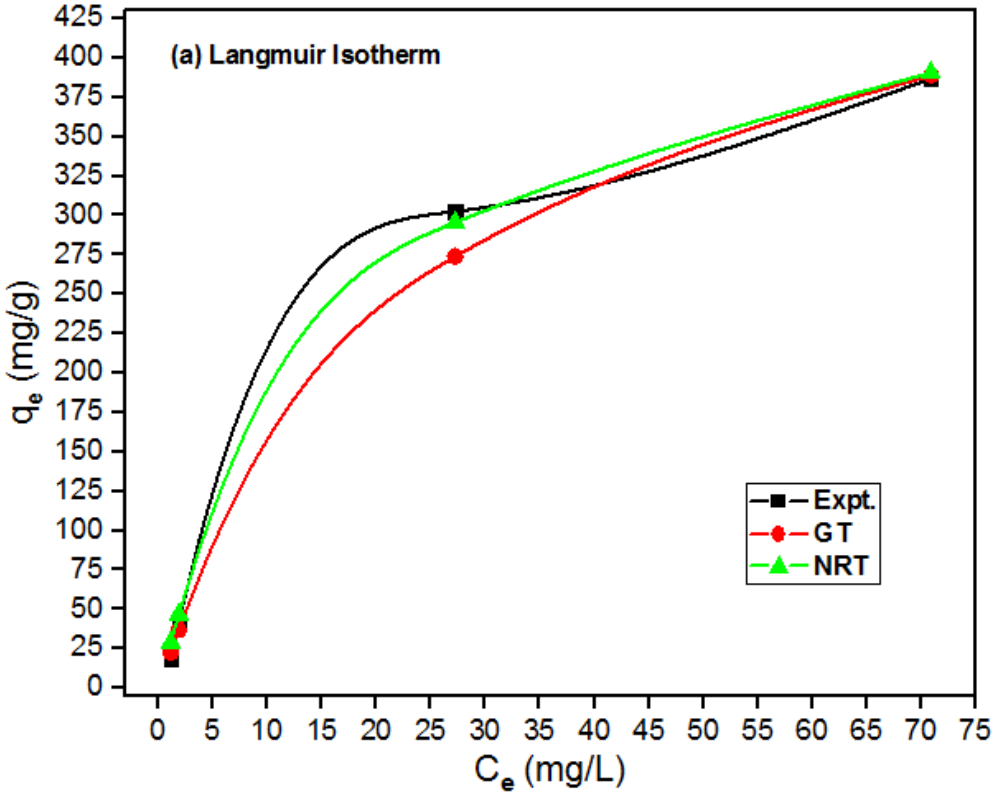
(a) Langmuir Isotherm
q_e (mg/g)
C_e (mg/L)
Expt.
GT
NRT

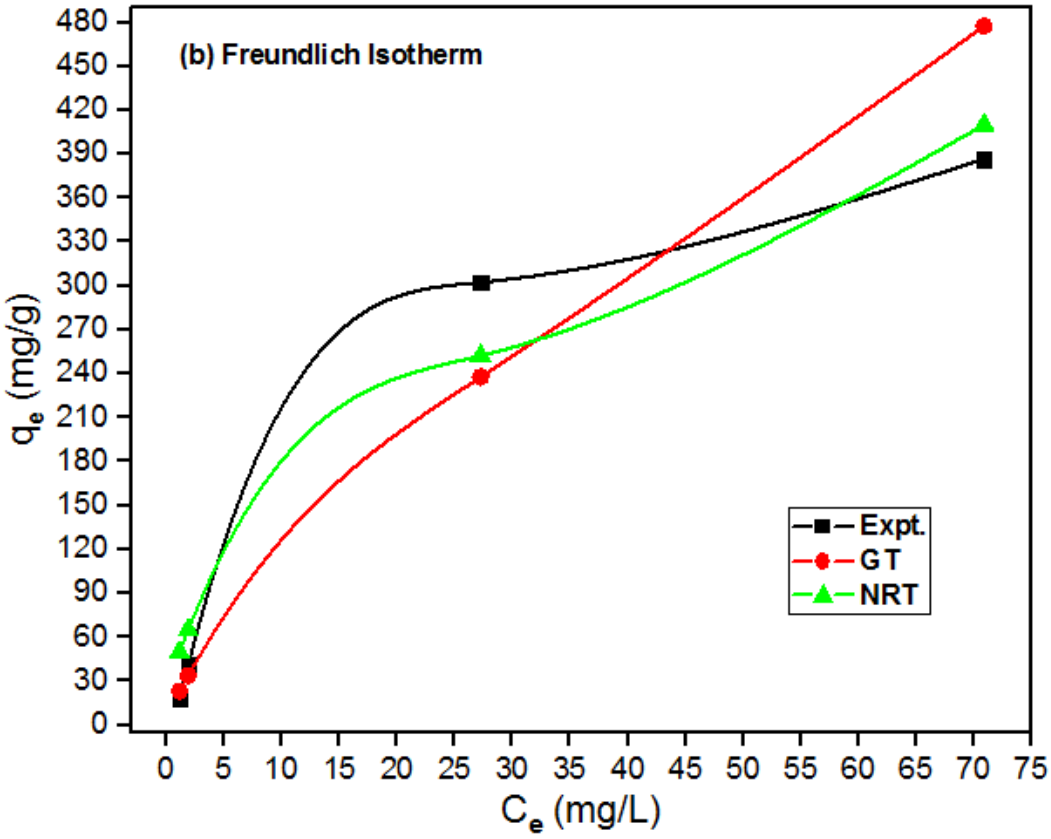
(b) Freundlich Isotherm
q_e (mg/g)
C_e (mg/L)
Expt.
GT
NRT

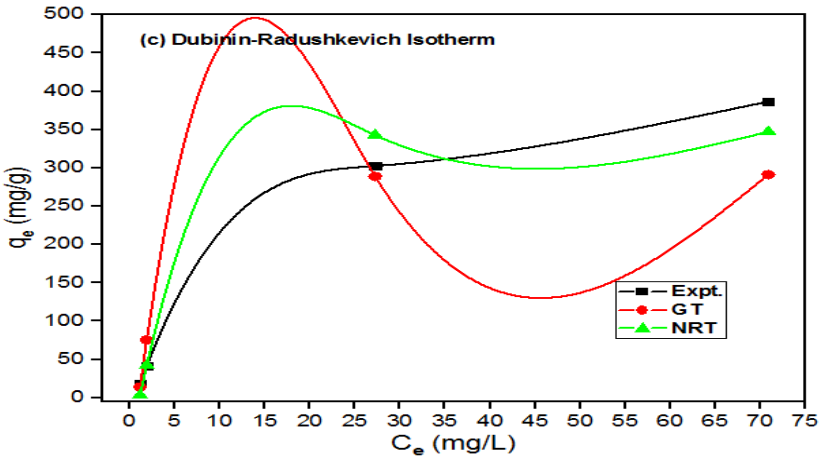

Figure-9: NRT, GT and Experimental Uptake Multiple Fits for (a) Langmuir, (b) Freundlich and (c) D-R Isotherms.

As shown in Figure 9 (a-c), the method line that is much closer to the observed line (black line) is the best method for that particular isotherm. In terms of proximity, the Langmuir curve under the 3 models is closest, followed by Freundlich and lastly the D-R curves. This indicates that the Langmuir model gave adequate prediction of the uptake of Cd under both GT and NRT solution schemes. Overall, the green curve, based on the NRT almost or partially fit the experimental black line. It is deduced that the NRT scheme of finding the isotherm parameters (q_{max}, K, n, b, and B) in all the models used is the most accurate for the observed data. Hence, the statistical results of the graphs in Figure-9, as shown in Table-9, can be utilized for model selection as well as choosing the best solution method.

Table-9: Statistical and Isotherm Parameters Obtained Using NRT (or Method B).

Isotherm Parameter	Langmuir	Freundlich	D-R
q_{max} (mg/g)	488.43147	-	347.88826
b	0.05624	-	-
K	-	47.15644	-
n	-	1.97052	-
B	-	-	1.78402
E (kJ/mol)	-	-	0.374343
Statistical Parameter			
R^2	0.99803	0.95516	0.9668
Adj. R^2	0.99705	0.93274	0.9502
Reduced Chi-Sqr.	101.1702	2305.59115	1707.06707
Residual Sum of Squares	202.3404	4611.1823	3414.13414

The Residual Sum of Squares (RSS) of 202.3404 in Table-9 shows a fairly good agreement between the Langmuir model and the experimental data. Thus, it can be said that Langmuir model is a good fit for describing and predicting biosorption of Cd using mango seed endocarp. Simply because it has the lowest RSS compared to Freundlich with 4611.1823 and D-R having 3414.134. In that case, the best fit to the experimental data are in the order of Langmuir, D-R and Freundlich isotherm model based on their RSS. In a similar fashion, the model with the lowest Reduced Chi-Square (χ^2) value is the best model, of which the ranking using RSS in the foregone stays the same. R^2 for all models from the GT are smaller compared to their corresponding values under NRT. This proves the effectiveness of the NRT scheme in estimating the uptake of metal as well as the isotherm parameters above GT. From the highest R^2 value to the least value: 0.99803, 0.9668 and 0.95516, the model rating starting with the best, is in the order of Langmuir, D-R and Freundlich. It explains clearly the reason for close and deviating fits in Figure-9. Amidst all the 3 models, the best fit to describe the biosorption of Cd metal using mango seed endocarp is the Langmuir model. However, to add on the missing piece, the parameter 'E', calculated and shown in Table-7 and 9 under D-R should pinpoint whether the adsorption follows a physical process or not. Magnitude of E between 8-16 kJ mol^{-1} implies that the adsorption process follows a chemical ion exchange, and a value of E < 8 kJ mol^{-1} hint at a physical nature. In view of that, estimates after GT and NRT gives E = 0.467678 & 0.374343kJ/mol respectively, implying a physical adsorption process of Cd onto the mango seed shell endocarp.

Kinetic Models: Time-dependent rate study data used in finding the unknown adsorption kinetic parameter in Pseudo-First order, Second order and an IPD models is shown in columns 1 and 2 of Table-10. This facilitates the calculation of all dependent and independent variables values from the linearized version of the model, as evident in the remaining 6 columns.

Employing Equations 10-14, parameters for each kinetic model can be evaluated using linear regression technique in Microsoft Excel, based on Table-10. Because the first 2 cells of $\log(q_e - q_t)$ column is empty due to undefined value obtained from our

computation, it is in line with Sahoo & Prelot assertion that the Lagergren equation is valid only for limited time range and it is impossible to extrapolate the empirical data to infinite time to get q_e. Thus, only 74% fit was achieved, as shown in Figure-10a.

On the other hand, Lagergren B model obtained from literature displays a better fit, as over 93% of the points falls on the straight line. As such, if the observed contact time is out of the range supported by the Lagergren A kinetic model, the 'B' equation may be used to determine the unknown parameters, as illustrated in Figure-10b. Thus, it can be said that Pseudo-First-Order 'B model' is a fairly good fit for describing and predicting the time-dependence of biosorption of Cd using mango seed endocarp. After a successful graphical representation, the model parameters obtained are presented in Table-11.

With an R^2 = 0.9978, the Second order kinetic model gives almost an excellent fit in agreement with the experimental data. The degree of agreement is shown by the Second Order plot of Figure-11a. Thus, it can be said that the Second Order model is better in terms of good fit for describing and predicting the time-dependence of biosorption of Cd using mango seed endocarp, as against the First Order equation. Plotting q_t against $\sqrt{t}$(Figure-9b) can be used to determine whether the IPD is the rate-limiting step. If the plot is linear and passes through the origin, it suggests that IPD is the sole rate-limiting step.

Table-10: Experimental Data andAxis Values from Linearized Kinetic Models Selected.

t	q_t	q_e	$\log(q_e - q_t)$	$\log q_e$	t/q_t	$t^{\frac{1}{2}}$	$1/q_t$
10	54.98	18.35	-	1.263636	0.181884	3.162278	0.018188
30	48.44	41.48695	-	1.617912	0.619323	5.477226	0.020644
60	46.42	302.509	2.408391	2.480738	1.292546	7.745967	0.021542
120	41.62	386.6797	2.537894	2.587351	2.883229	10.95445	0.024027

Units: t (min); q_t(mg/g); q_e(mg/g); t/q_t (ming/mg); $t^{\frac{1}{2}}$ (min^{½}) and;$1/q_t$ (g/mg).

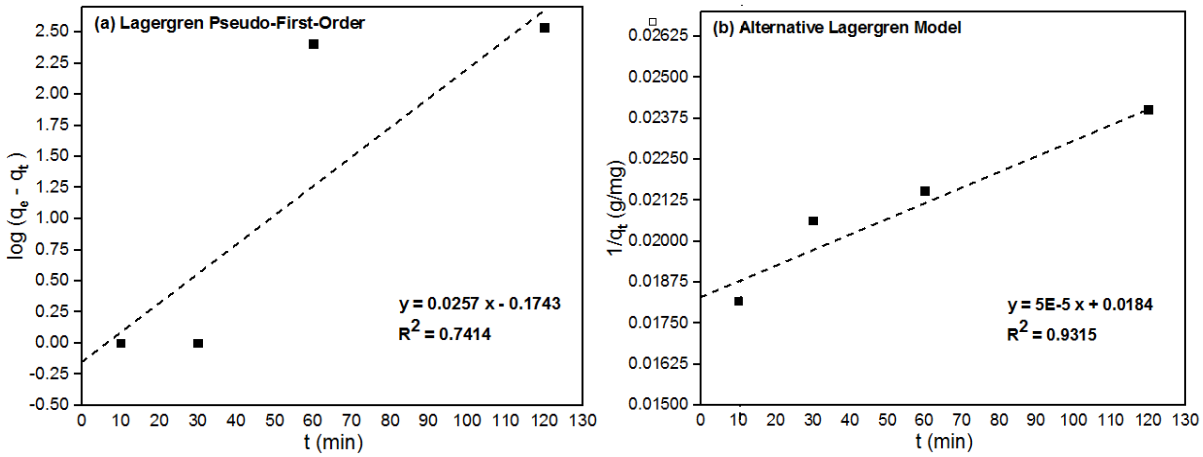

Figure-10: Kinetic Parameters from Two Different Versions of the Lagergren Model.

Table-11: Calculated Parameters of the Nonlinear Form of First Order Kinetic Model.

Parameter	Model			
	Lagergren A	Lagergren B	Second Order	IPD Model
q_e (mg/g)	0.840045	54.34783	40.48583	-
k_1 (min^{-1})	0.059187	0.002717	-	-
k_2 g/ (mg min)$^{-1}$	-	-	-0.005423	-
k_d (mg/g min$^{-1/2}$)	-	-	-	-1.6285
R^2	0.7414	0.9315	0.9978	0.9546

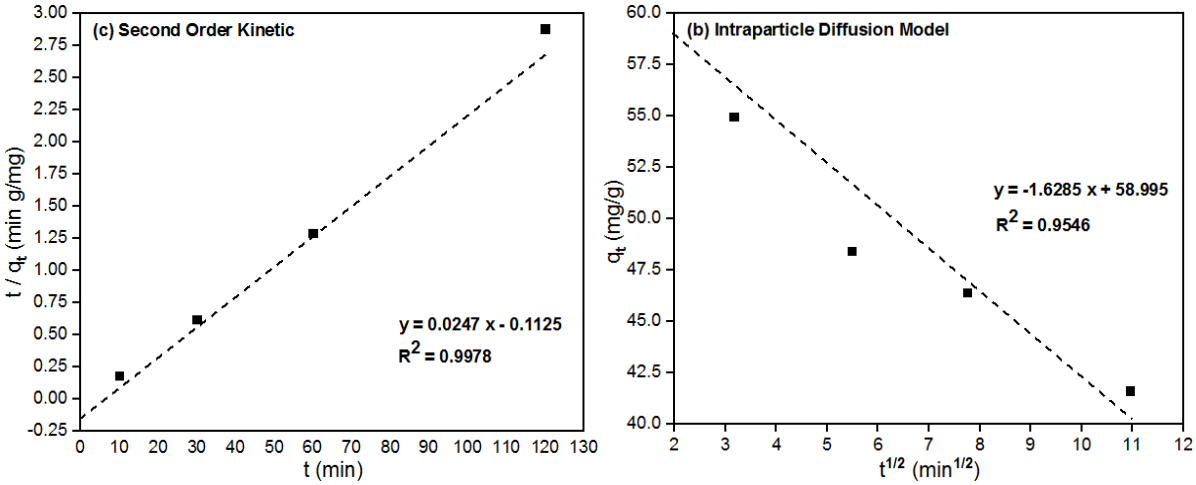

Figure-11: Graphical Representation of (a) Second Order and (b) IPD Model Kinetic Parameters.

However, if the plot exhibits multiple linear segments as shown in Figure-11b, it implies that other factors, such as film diffusion or adsorption equilibrium, may also be influencing the process. An intercept value of 58.995 changes Equation 12 to Equation-16.

$$q_t = k_d t^{0.5} + C_d \quad (16)$$

In this case, C_d = 58.995 mg/g stands for thickness of the boundary layer. It is important to note that the value of C_d is not limited to a specific range. Though larger C_d implies the greater effect of the boundary layer[46]. The magnitude of C_d can vary significantly based on several factors, including: solute and adsorbent properties, initial concentration, particle size, agitation and mixing and temperature. Higher C_i leads to larger values of C_d and smaller particles may lead to smaller values of C_d. A negative value for k_d(–1.6285 mg/g $min^{-½}$) would indicate that the model is not appropriate for describing the adsorption process under those conditions. Because it means that the solute molecules are diffusing out of the adsorbent particles over time, which contradicts the fundamental concept of adsorption, where molecules are expected to be adsorbed onto the adsorbent surface or within its pores. Thus, it can be said that the IPD model is not a good fit for describing and predicting the time-dependence of biosorption of Cd using mango seed endocarp. From the plots examined (Figure-8 and 9), the closest fit to the time dependent biosorption study data is the Second order kinetic equation followed by the Pseudo-First-Order B model.

Conclusion

Sorption of Cd^{2+} was investigated in a batch system using powdered mango seed shell endocarp as potential adsorbent prepared in the laboratory. By differing contact time, dosage, initial biosorbent concentration and pH in 4 runs, the final Cd^{2+} concentration was determined for each of the respective variations using AAS to facilitate the calculation of the percent biosorption. The maximum biosorption rate (efficiency) of 82.47%, 99.49%, 62.43% and 62.45% achieved, occur at 10 min, 0.5g mango shell dosage, 5 mg/L initial Cd^{2+} concentration and a pH of 4, respectively. Further test of the experimental process data by carrying out adsorption isotherm study using Langmuir, Freundlich and D-R models, shows that the Langmuir isotherm equations performs better statistically. Linear graphical representation to predict kinetic parameters in Lagergren, alternative Lagergren, Pseudo Second order and the IPD adsorption kinetic models, results in k_1 & q_e of 0.0592 min^{-1} & 0.84mg/g; k_1 & q_e of 0.0027 min^{-1} & 54.348mg/g; k_2 & q_e equal to –0.0054g/(mg $min)^{-1}$ & 40.4858mg/g and; k_d = –1.6285 mg/g $min^{-½}$, respectively – base on which the Second order kinetic gave the closest fit. Subsequent study should look at the chemical treatment and activation of the mango seed shell epicarp biosorbent for optimal adsorption capability. Other kinetic models like the zero-order, nth order, Bhattacharya and Venkobachar, Natarajan and Khalaf, Elovich and Boyd kinetic models should be used to fit the biosorption data since the Lagergren Model A and the IPD kinetic model did not sufficiently describe the biosorption kinetics. It is also important to rank the best isotherm models by including the Weber and Morris, Flory-Huggins, Redlich-Peterson, Vieth-Sladek and Temkin isotherm models to the one selected for this study.

References

1. Zhuang, P., McBride, M. B., Xia, H., Li, N., & Li, Z. (2009). Health risk from heavy metals via consumption of food crops in the vicinity of Dabaoshan mine, South China. *Science of the total environmen*t, 407(5), 1551-1561.

2. Sarı, A., & Tuzen, M. (2008). Biosorption of cadmium (II) from aqueous solution by red algae (Ceramium virgatum): equilibrium, kinetic and thermodynamic studies. *Journal of hazardous materials*, 157(2-3), 448-454.

3. Smith J.E. (2012). Biotechnology-Studies in Biology. 4th ed. Cambridge University Press; 2012.

doi:10.1017/CBO9781139167215

4. Rahimzadeh, M. R., Rahimzadeh, M. R., Kazemi, S., & Moghadamnia, A. A. (2017). Cadmium toxicity and treatment: An update. *Caspian journal of internal medicine*, 8(3), 135.

5. Tucker, P. (2011). Agency for toxic substances and disease registry. *Case Studies in Environmental Medicine: Asbestos Toxicity*.

6. WHO (2019). Exposure to Cadmium: A Major Public Health Concern. Team-Chemical Safety and Health Unit; https://www.who.int/publications-detail-redirect/WHO-CED-PHE-EPE-19-4-3

7. Pinto, A. P., Mota, A. D., De Varennes, A., & Pinto, F. C. (2004). Influence of organic matter on the uptake of cadmium, zinc, copper and iron by sorghum plants. *Science of the total environment*, 326(1-3), 239-247.

8. Goyer, R. A., & Clarkson, T. W. (1996). Toxic effects of metals. *Casarett and Doull's toxicology: the basic science of poisons*, 5, 691-736.

9. Mata, Y. N., Blázquez, M. L., Ballester, A., González, F., & Munoz, J. A. (2009). Biosorption of cadmium, lead and copper with calcium alginate xerogels and immobilized Fucus vesiculosus. *Journal of hazardous materials*, 163(2-3), 555-562.

10. Montazer-Rahmati, M. M., Rabbani, P., Abdolali, A., & Keshtkar, A. R. (2011). Kinetics and equilibrium studies on biosorption of cadmium, lead, and nickel ions from aqueous solutions by intact and chemically modified brown algae. *Journal of hazardous materials*, 185(1), 401-407.

11. Pradhan, A. A., & Levine, A. D. (1992). Role of extracellular components in microbial biosorption of copper and lead. *Water Science and Technology*, 26(9-11), 2153-2156.

12. Sharma, Y. C. (1995). Economic treatment of cadmium (II)-rich hazardous waste by indigenous material. *Journal of colloid and interface science*, 173(1), 66-70.

13. Rao, K. S., Mohapatra, M., Anand, S., & Venkateswarlu, P. (2010). Review on cadmium removal from aqueous solutions. *International journal of engineering, science and technology*, 2(7).

14. Yun, Y. S., & Volesky, B. (2003). Modeling of lithium interference in cadmium biosorption. *Environmental science & technology*, 37(16), 3601-3608.

15. Kurniawan, T. A., Chan, G. Y., Lo, W. H., & Babel, S. (2006). Comparisons of low-cost adsorbents for treating wastewaters laden with heavy metals. *Science of the total environment*, 366(2-3), 409-426.

16. Hameed, B. H., Mahmoud, D. K., & Ahmad, A. L. (2008). Sorption equilibrium and kinetics of basic dye from aqueous solution using banana stalk waste. *Journal of Hazardous Materials*, 158(2-3), 499-506.

17. Raval, N. P., Shah, P. U., & Shah, N. K. (2016). Adsorptive removal of nickel (II) ions from aqueous environment: A review. *Journal of environmental management*, 179, 1-20.

18. Fane, A. G., Awang, A. R., Bolko, M., Macoun, R., Schofield, R., Shen, Y. R., & Zha, F. (1992). Metal recovery from wastewater using membranes. *Water Science and Technology*, 25(10), 5-18.

19. Benvenuti, T., Krapf, R. S., Rodrigues, M. A. S., Bernardes, A. M., & Zoppas-Ferreira, J. (2014). Recovery of nickel and water from nickel electroplating wastewater by electrodialysis. *Separation and purification technology*, 129, 106-112.

20. Jakobsen, M. R., Fritt-Rasmussen, J., Nielsen, S., & Ottosen, L. M. (2004). Electrodialytic removal of cadmium from wastewater sludge. *Journal of Hazardous Materials*, 106(2-3), 127-132.

21. Qdais, H. A., & Moussa, H. (2004). Removal of heavy metals from wastewater by membrane processes: a comparative study. Desalination, 164(2), 105-110.

22. Saffaj, N., Loukili, H., Younssi, S. A., Albizane, A., Bouhria, M., Persin, M., & Larbot, A. (2004). Filtration of solution containing heavy metals and dyes by means of ultrafiltration membranes deposited on support made of Moroccan clay. *Desalination*, 168, 301-306.

23. Danesi, P. R. (1984). Separation of metal species by supported liquid membranes. *Separation Science and Technology*, 19(11-12), 857-894.

24. Kumar, V., Sahu, S. K., & Pandey, B. D. (2010). Prospects for solvent extraction processes in the Indian context for the recovery of base metals. A review. *Hydrometallurgy*, 103(1-4), 45-53.

25. Provazi, K., Campos, B. A., Espinosa, D. C. R., & Tenório, J. A. S. (2011). Metal separation from mixed types of batteries using selective precipitation and liquid–liquid extraction techniques. *Waste Management*, 31(1), 59-64.

26. Jha, M. K., Kumar, V., Jeong, J., & Lee, J. C. (2012). Review on solvent extraction of cadmium from various solutions. *hydrometallurgy*, 111, 1-9.

27. Tzanetakis, N., Taama, W. M., Scott, K., Jachuck, R. J. J., Slade, R. S., & Varcoe, J. (2003). Comparative performance of ion exchange membranes for electrodialysis of nickel and cobalt. *Separation and Purification Technology*, 30(2), 113-127.

28. Otrembska, P., & Gęga, J. (2012). Separation of nickel (II) and cadmium (II) with ion-exchange process. *Separation Science and Technology*, 47(9), 1345-1349.

29. Papadopoulos, A., Fatta, D., Parperis, K., Mentzis, A., Haralambous, K. J., & Loizidou, M. (2004). Nickel uptake from a wastewater stream produced in a metal finishing

industry by combination of ion-exchange and precipitation methods. *Separation and Purification Technology*, 39(3), 181-188.

30. Tünay, O., & Kabdaşli, N. I. (1994). Hydroxide precipitation of complexed metals. *Water Research*, 28(10), 2117-2124.

31. Lazaridis, N. K., & Asouhidou, D. (2003). Kinetics of sorptive removal of chromium (VI) from aqueous solutions by calcined Mg–Al–CO_3 hydrotalcite. *Water research*, 37(12), 2875-2882.

32. Hawari, A. H., & Mulligan, C. N. (2006). Biosorption of lead (II), cadmium (II), copper (II) and nickel (II) by anaerobic granular biomass. *Bioresource technology*, 97(4), 692-700.

33. Mukherjee, S. K., & Litz, R. E. (2009). Introduction: botany and importance. In The mango: Botany, production and uses (pp. 1-18). Wallingford UK: CABI.

34. Arogba, S. S. (1997). Physical, chemical and functional properties of Nigerian mango (Mangifera indica) kernel and its processed flour. *Journal of the Science of Food and Agriculture*, 73(3), 321-328.

35. Ramteke, R. S., & Eipeson, W. E. (1997). Effect of additives on the stability of mango aroma concentrate during storage. *Journal of Food Science and Technology*, 34(3), 195-199.

36. Sogi, D. S., Siddiq, M., Greiby, I., & Dolan, K. D. (2013). Total phenolics, antioxidant activity, and functional properties of 'Tommy Atkins' mango peel and kernel as affected by drying methods. *Food chemistry*, 141(3), 2649-2655.

37. Murugan, T., Ganapathi, A., & Valliappan, R. (2010). Removal of dyes from aqueous solution by adsorption on biomass of mango (Mangifera indica) leaves. *Journal of Chemistry*, 7, 669-676.

38. Ashraf, M. A., Wajid, A., Mahmood, K., Maah, M. J., & Yusoff, I. (2011). Removal of heavy metals from aqueous solution by using mango biomass. *African Journal of Biotechnology*, 10(11), 2163-2177.

39. Iqbal, M., Saeed, A., & Zafar, S. I. (2009). FTIR spectrophotometry, kinetics and adsorption isotherms modeling, ion exchange, and EDX analysis for understanding the mechanism of Cd^{2+} and Pb^{2+} removal by mango peel waste. *Journal of hazardous materials*, 164(1), 161-171.

40. Kowanga, K. D., Gatebe, E., Mauti, G. O., & Mauti, E. M. (2016). Kinetic, sorption isotherms, pseudo-first-order model and pseudo-second-order model studies of Cu (II) and Pb (II) using defatted Moringa oleifera seed powder. *The journal of phytopharmacology*, 5(2), 71-78.

41. Khayyun, T. S., & Mseer, A. H. (2019). Comparison of the experimental results with the Langmuir and Freundlich models for copper removal on limestone adsorbent. *Applied Water Science*, 9(8), 170.

42. Musah, M., Azeh, Y., Mathew, J. T., Umar, M. T., Abdulhamid, Z., & Muhammad, A. I. (2022). Adsorption kinetics and isotherm models: a review. *CaJoST*, 4(1), 20-26.

43. Okeola, F. O., & Odebunmi, E. O. (2010). Comparison of Freundlich and Langmuir isotherms for adsorption of methylene blue by agrowaste derived activated carbon. *Advances in Environmental Biology*, 329-336.

44. Thang, N. H., Khang, D. S., Hai, T. D., Nga, D. T., & Tuan, P. D. (2021). Methylene blue adsorption mechanism of activated carbon synthesised from cashew nut shells. *RSC advances*, 11(43), 26563-26570.

45. Revellame, E. D., Fortela, D. L., Sharp, W., Hernandez, R., & Zappi, M. E. (2020). Adsorption kinetic modeling using pseudo-first order and pseudo-second order rate laws: A review. *Cleaner Engineering and Technology*, 1, 100032.

46. Sahoo, T. R., & Prelot, B. (2020). Adsorption processes for the removal of contaminants from wastewater: the perspective role of nanomaterials and nanotechnology. *In Nanomaterials for the detection and removal of wastewater pollutants*, pp. 161-222. Elsevier.